

# The unifying theory of scaling in thermal convection: the updated prefactors

Richard J. A. M. Stevens<sup>1,2,†</sup>, Erwin P. van der Poel<sup>2</sup>, Siegfried Grossmann<sup>3</sup>  
and Detlef Lohse<sup>2,†</sup>

<sup>1</sup>Department of Mechanical Engineering, Johns Hopkins University, Baltimore, MD 21218, USA

<sup>2</sup>Physics of Fluids Group, Faculty of Science and Technology, J.M. Burgers Center for Fluid Dynamics, and MESA+ Institute, University of Twente, 7500 AE Enschede, The Netherlands

<sup>3</sup>Fachbereich Physik, Philipps-Universität Marburg, Am Renthof 6, D-35032 Marburg, Germany

(Received 29 January 2013; revised 9 May 2013; accepted 6 June 2013)

The unifying theory of scaling in thermal convection (Grossmann & Lohse, *J. Fluid Mech.*, vol. 407, 2000, pp. 27–56; henceforth the GL theory) suggests that there are no pure power laws for the Nusselt and Reynolds numbers as function of the Rayleigh and Prandtl numbers in the experimentally accessible parameter regime. In Grossmann & Lohse (*Phys. Rev. Lett.*, vol. 86, 2001, pp. 3316–3319) the dimensionless parameters of the theory were fitted to 155 experimental data points by Ahlers & Xu (*Phys. Rev. Lett.*, vol. 86, 2001, pp. 3320–3323) in the regime  $3 \times 10^7 \leq Ra \leq 3 \times 10^9$  and  $4 \leq Pr \leq 34$  and Grossmann & Lohse (*Phys. Rev. E*, vol. 66, 2002, p. 016305) used the experimental data point from Qiu & Tong (*Phys. Rev. E*, vol. 64, 2001, p. 036304) and the fact that  $Nu(Ra, Pr)$  is independent of the parameter  $a$ , which relates the dimensionless kinetic boundary thickness with the square root of the wind Reynolds number, to fix the Reynolds number dependence. Meanwhile the theory is, on the one hand, well-confirmed through various new experiments and numerical simulations; on the other hand, these new data points provide the basis for an updated fit in a much larger parameter space. Here we pick four well-established (and sufficiently distant)  $Nu(Ra, Pr)$  data points and show that the resulting  $Nu(Ra, Pr)$  function is in agreement with almost all established experimental and numerical data up to the ultimate regime of thermal convection, whose onset also follows from the theory. One extra  $Re(Ra, Pr)$  data point is used to fix  $Re(Ra, Pr)$ . As  $Re$  can depend on the definition and the aspect ratio, the transformation properties of the GL equations are discussed in order to show how the GL coefficients can easily be adapted to new Reynolds number data while keeping  $Nu(Ra, Pr)$  unchanged.

**Key words:** Bénard convection, turbulent convection, turbulence theory

---

## 1. Introduction

Thermal convection is omnipresent in science and technology and its paradigmatic representation is Rayleigh–Bénard (RB) convection: a fluid in a sample heated from below and cooled from above. This system has received considerable attention in the

† Email addresses for correspondence: [r.j.a.m.stevens@utwente.nl](mailto:r.j.a.m.stevens@utwente.nl), [d.lohse@utwente.nl](mailto:d.lohse@utwente.nl)

few last decades (Siggia 1994; Ahlers, Grossmann & Lohse 2009b; Lohse & Xia 2010), with one focus on the scaling properties of the global heat transport of the system. The now widely accepted viewpoint is the Grossmann–Lohse (GL) theory (Grossmann & Lohse 2000, 2001, 2002, 2004). The basis for this theory of scaling in RB convection are exact global balances for the energy and thermal dissipation rates derived from the Boussinesq equations and the decomposition of the flow in boundary layer (BL) and bulk contributions. The scaling of the dissipation rates in the BLs is assumed to obey Prandtl–Blasius–Pohlhausen scaling (Schlichting 1979), which is justified as long as the shear-Reynolds numbers of the BLs are not too large, and the scaling relations in the bulk are estimated based on Kolmogorov-type arguments for homogeneous isotropic turbulence. While the theory gives the different scaling relations for the individual contributions to the energy dissipation rates in the bulk and in the BL, namely  $\epsilon_{u,bulk}$  and  $\epsilon_{u,BL}$ , and to the thermal dissipation rates in the bulk (background) and in the BLs (plus the plumes, see Grossmann & Lohse (2004)), namely  $\epsilon_{\theta,bulk}$  and  $\epsilon_{\theta,BL}$ , the absolute sizes of these four relative contributions are not given by the theory. They are expressed in four dimensionless prefactors  $c_i$ ,  $i = 1, 2, 3, 4$ , for  $\epsilon_{u,BL}$ ,  $\epsilon_{u,bulk}$ ,  $\epsilon_{\theta,BL}$  and  $\epsilon_{\theta,bulk}$ , respectively, which have to be obtained from experimental or numerical data for  $Nu(Ra, Pr)$ .

When the theory was developed in the early 21st century, such data were scarce and often contradicting each other, due to sidewall and plate effects, insufficient knowledge of the material properties of the fluid, lack of numerical resolution and other problems. Grossmann & Lohse (2001) used 155 data points for  $Nu(Ra, Pr)$  in the parameter range  $3 \times 10^7 \leq Ra \leq 3 \times 10^9$  and  $4 \leq Pr \leq 34$  obtained by Ahlers & Xu (2001), which was the most extensive data set at that time. This fixed  $Nu(Ra, Pr)$  for all  $Ra$  and  $Pr$ , considered as valid up to the meanwhile found (He *et al.* 2012b) ultimate regime of thermal convection, where the Prandtl–Blasius-type BL becomes unstable. Here  $Re(Ra, Pr)$  was fixed (cf. Grossmann & Lohse 2002) with one extra adoption of the prefactor  $a$ , i.e. the amplitude parameter of the Prandtl BL thickness, in the Prandtl–Blasius scaling relation  $\lambda_u = aL/\sqrt{Re}$ , to the experimental data of Qiu & Tong (2001), where  $\lambda_u$  is the mean thickness of the kinetic BL and  $L$  the height of the sample.

Although the data to which we adopted the four prefactors  $c_i$  and  $a$  were relatively local in parameter space, the theory was rather successful in describing the global behaviour of  $Nu(Ra, Pr)$  and  $Re(Ra, Pr)$ , as described in detail by Ahlers *et al.* (2009b). This included the prediction that for  $Pr \approx 1$  the onset to the ultimate regime should take place when  $Ra$  is of the order of  $10^{14}$ . This prediction was based on an assumed onset of a sheared BL instability at a shear Reynolds number  $Re_s \approx 420$ , which is the value given by Landau & Lifshitz (1987). Indeed, very recently He *et al.* (2012b) have found the onset of the ultimate regime at this very Rayleigh number. Thanks to joint efforts of the community the experimental and numerical data situation for  $Nu(Ra, Pr)$  has considerably improved in the last decade. Measurements have been extended to a much larger domain in the  $Ra$ – $Pr$  parameter space, see the updated phase diagrams in figures 1 and 8, and plate and sidewall corrections are much better understood and taken into account (Ahlers 2000; Roche *et al.* 2001; Verzicco 2002; Niemela & Sreenivasan 2003; Brown *et al.* 2005; Ahlers *et al.* 2009b). One notices that for  $\Gamma = 1/2$  higher  $Ra$  number values have been obtained than for  $\Gamma = 1$ , while the  $Pr$  number dependence is much more explored for  $\Gamma = 1$  than for  $\Gamma = 1/2$ . Furthermore, due to the increasing computational power and better codes the numerical data are now well converged, confirming and complementing the experimental data. Meanwhile Stevens, Verzicco & Lohse (2010c) and Stevens, Lohse

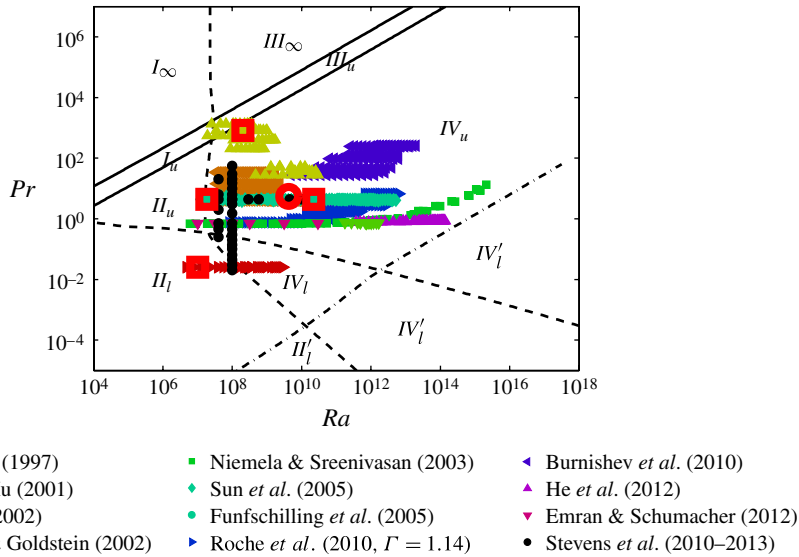


FIGURE 1. (Colour online) Phase diagram in  $Ra$ - $Pr$  plane for RB convection according to the GL model (Grossmann & Lohse 2000, 2001, 2002, 2004) in a  $\Gamma = 1$  sample with no-slip boundary conditions. The upper solid line means  $Re = 1$ ; the lower nearly parallel solid line corresponds to  $\epsilon_{u,BL} = \epsilon_{u,bulk}$ ; the curved solid and dashed line is  $\epsilon_{\theta,BL} = \epsilon_{\theta,bulk}$ ; and along the long-dashed line  $\lambda_u = \lambda_\theta$ , i.e.  $2aNu = \sqrt{Re}$ . The dash-dotted line indicates where the laminar kinetic BL is expected to become turbulent, based on a critical shear Reynolds number  $Re_s^* = 1014$  of the kinetic BL: see the text. The data are from Cioni, Ciliberto & Sommeria (1997), Glazier *et al.* (1999), Ahlers & Xu (2001), Chaumat, Castaing & Chilla (2002), Fleischer & Goldstein (2002), Xia, Lam & Zhou (2002), Niemela & Sreenivasan (2003), Funfschilling *et al.* (2005), Sun *et al.* (2005), Burnishev, Segre & Steinberg (2010), Roche *et al.* (2010), Stevens, Clercx & Lohse (2010*a,b*), Emran & Schumacher (2012), He *et al.* (2012*a*) and van der Poel, Stevens & Lohse (2013). Note that for the Stevens *et al.* data, points from different papers have been combined in the graph. The four large open squares (shown in red online) indicate the location of the four  $Nu(Ra, Pr)$  points and the large open circle (shown in red online) indicates the  $Re(Ra, Pr)$  point that has been used for the new GL fit.

& Verzicco (2011*a*) achieved  $Ra = 2 \times 10^{12}$  at  $Pr = 0.7$  in a  $\Gamma = 1/2$  sample and obtained a good agreement with the experimental data of Niemela *et al.* (2000) and He *et al.* (2012*b*).

This situation calls for a refit of the four prefactors  $c_i$  and  $a$  of the GL theory, in spite of the success of the theory with the coefficients of Grossmann & Lohse (2001): it is clear that the surface  $Nu(Ra, Pr)$  above the  $Ra$ - $Pr$  parameter space will be much more stable and ‘wobble’ less if we put it on four distant and trustable ‘legs’  $Nu_i(Ra_i, Pr_i)$ ,  $i = 1, 2, 3, 4$ , rather than putting it on four ‘legs’ somewhere in the centre but close to each other. As we will see  $Nu(Ra, Pr)$  is only determined by the choice of these four  $Nu(Ra, Pr)$  data points from experiments. The accuracy of the GL fit is verified by comparing it with several data sets over a wide parameter regime and by making a second fit that reveals in which regimes there is some uncertainty. Including more data points in the fitting procedure does not lead to better fits since data tend to be clustered in the phase space. Therefore, including more data points increases the weight of some data without actually adding additional physical

information. An additional Reynolds number measurement is necessary to fix  $a$  and the relation between  $a$  and  $Re_L$ , which is the Reynolds number for which no bulk is left and the whole flow consists of laminar BL as will be explained below. The shortcoming of the old set of  $c_i$ ,  $a$  and  $Re_L$  was particularly obvious for small  $Pr$ , say  $Pr \leq 1$  (see figure 5), because in the days of Grossmann & Lohse (2001) no reliable information was available in that parameter regime and therefore no Nusselt data of that regime had been included in the fit.

The structure of this paper is as follows: in § 2 we will provide the refit of the GL theory for an aspect ratio  $\Gamma = 1$ , leading to  $Nu(Ra, Pr)$  in the whole parameter space up to the ultimate state. In § 3 we discuss the robustness of the fit. In § 4 we will show that this fit also describes the available data for  $\Gamma = 1/2$  and will in particular discuss the onset of the ultimate regime. Section 5 gives conclusions and an outlook on the new challenges.

## 2. Refit of the GL theory for $\Gamma = 1$

The GL theory describes  $Nu(Ra, Pr)$  and  $Re(Ra, Pr)$  with the following two coupled equations (Ahlers *et al.* 2009b),

$$(Nu - 1)RaPr^{-2} = c_1 \frac{Re^2}{g(\sqrt{Re_L/Re})} + c_2 Re^3, \quad (2.1)$$

$$Nu - 1 = c_3 Re^{1/2} Pr^{1/2} \left\{ f \left[ \frac{2aNu}{\sqrt{Re_L}} g \left( \sqrt{\frac{Re_L}{Re}} \right) \right] \right\}^{1/2} + c_4 Pr Re f \left[ \frac{2aNu}{\sqrt{Re_L}} g \left( \sqrt{\frac{Re_L}{Re}} \right) \right], \quad (2.2)$$

where the cross-over functions  $f$  and  $g$  model the cross-over from the thermal BL nested in the kinetic one towards the inverse situation and that for which  $\lambda_u \sim L$  loses its scaling with  $Re$  since  $\lambda_u$  extends to sample half-height  $L/2$  and cannot increase further with decreasing  $Re$ ; for details see Grossmann & Lohse (2001). As described by Grossmann & Lohse (2002) the prefactor  $a$  has to be determined from experimental data. Whereas the definition of the Nusselt number is very clear there are various reasonable ways to define a Reynolds number. We decided to use one experimental data point of Qiu & Tong (2001) to determine the value of  $a$  and from figure 1 of Grossmann & Lohse (2002) we read  $Ra = 4.2 \times 10^9$ ,  $Pr = 5.5$ ,  $Re = 2.1 \times 10^3$ . In addition we demand for the Reynolds number  $Re_L$  that  $\lambda_u = aL/\sqrt{Re_L} = L/2$ , meaning that  $Re_L = (2a)^2$  is fixed for given  $a$ .

In order to obtain accurate values for the four dimensionless prefactors  $c_i$ , it is necessary to choose four data points with as much information on the richness of the RB system as possible, which means that data points from different regimes should be selected. Therefore we determined the  $c_i$  from the data points of Funfschilling *et al.* (2005) at  $Ra = 1.8 \times 10^7$  and  $Ra = 2.25 \times 10^{10}$ , both with  $Pr = 4.38$ , the data point from Xia *et al.* (2002) with  $Pr = 818$  at  $Ra = 2.04 \times 10^8$ , and the data point from Cioni *et al.* (1997) at  $Ra = 1 \times 10^7$  with  $Pr = 0.025$ . The location of these data points in the RB phase diagram is indicated by the large squares (shown in red online) in figure 1 and by the black dots in the corresponding three-dimensional  $Nu(Ra, Pr)$  visualization in figure 2(a). Figure 1 shows that these data are indeed within different regimes. The reason for choosing these specific data points is two-fold. First of all we consider these four data points to be reliable. And apart from the data point by Xia *et al.*

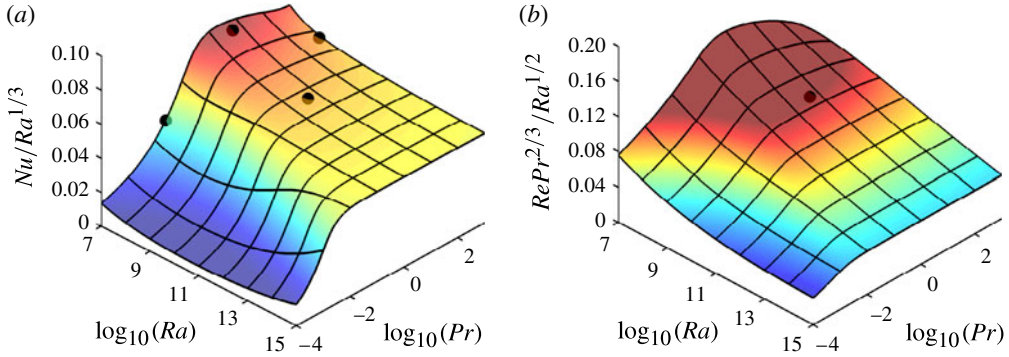


FIGURE 2. (Colour online) Compensated three-dimensional visualization of (a)  $Nu(Ra, Pr)$  and (b)  $Re(Ra, Pr)$ . The four  $Nu(Ra, Pr)$  points and the  $Re(Ra, Pr)$  point used to fit the GL parameters  $c_1 = 8.05$ ,  $c_2 = 1.38$ ,  $c_3 = 0.487$ ,  $c_4 = 0.0252$  have been indicated by the black points in the  $Nu(Ra, Pr)$  and  $Re(Ra, Pr)$  graph, respectively.

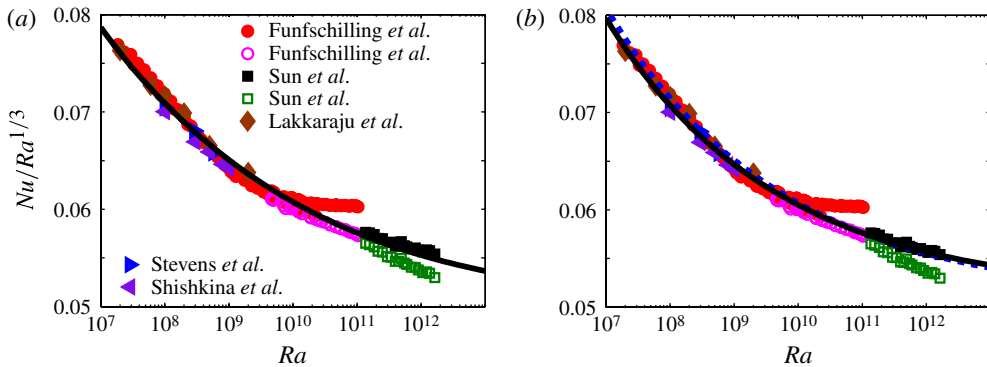


FIGURE 3. (Colour online) Comparison of the  $Ra$  scaling of the original GL fit from Grossmann & Lohse (2001) (a) with the new fit (b) for water, i.e.  $Pr = 4.38$  unless mentioned otherwise, in a  $\Gamma = 1$  sample. The circles (Funfschilling *et al.* 2005) and squares (Sun & Xia 2005) indicate experimental results. Open symbols indicate the uncorrected data and solid symbols the data after correction for the finite plate conductivity. The diamonds (Lakkaraju *et al.* (2012),  $Pr = 5.4$ ), right pointing triangles (Stevens *et al.* 2011b) and left pointing triangles (Shishkina & Thess 2009) indicate results from numerical simulations. The solid (black) line indicates the GL fit of § 2 and the dashed (shown in blue online) line the GL fit of § 3.

(2002), which is the only experiment in that large  $Pr$  regime, all data points agree very well with experimental or numerical data from other groups, see figures 3 and 5. In addition, these four data points are relatively far apart in the  $Ra$ – $Pr$  parameter space to ensure that they provide the theory with as much information on the richness of the RB physics as possible. To provide information on the  $Ra$  scaling we selected the measurements of Funfschilling *et al.* (2005) at  $Ra = 1.8 \times 10^7$  and  $Ra = 2.25 \times 10^{10}$  with  $Pr = 4.38$ . In order to include information on the transition between the ‘upper’ and ‘lower’ regimes, which is modelled by the cross-over functions  $f$  and  $g$ , it is necessary to include data points in the low-, intermediate- and high- $Pr$  regime. We do

this selecting next to the intermediate  $Pr$  number data from Funfschilling *et al.* (2005), the low  $Pr = 0.025$  number measurement by Cioni *et al.* (1997) at  $Ra = 1 \times 10^7$  and the high  $Pr = 818$  measurement by Xia *et al.* (2002) at  $Ra = 2.04 \times 10^8$ . Altogether the four data points provide information from three different  $Pr$  numbers and four different  $Ra$  numbers. From these four data points, and an initial guess for  $a$ , we determine the  $c_i$  with a Newton–Raphson root finding method or by using a trust-region-reflective optimization algorithm, which both give the same result. Subsequently, the  $Re(Ra, Pr)$  point of Qiu & Tong (2001) is used to find the appropriate value of  $a$  with the transformation property of the GL model (Grossmann & Lohse 2002), which is described below in detail. Owing to this transformation property of the GL equations the four  $Nu(Ra, Pr)$  data points determine the Nusselt number dependence, while the  $Re$  number data point of Qiu & Tong (2001) fixes the absolute value of the Reynolds number throughout the phase space. This results in the following five GL parameters  $c_1 = 8.05$ ,  $c_2 = 1.38$ ,  $c_3 = 0.487$ ,  $c_4 = 0.0252$  and  $a = 0.922$ . The difference in significant numbers is due to the fact that some coefficients are less sensitive to uncertainty than others.

It was pointed out by Grossmann & Lohse (2002) that  $Nu(Ra, Pr)$  is invariant and thus independent of the parameter  $a$  under the following transformation

$$Re \rightarrow \alpha Re, \quad (2.3)$$

$$a \rightarrow \alpha^{1/2} a, \quad (2.4)$$

$$c_1 \rightarrow c_1/\alpha^2, \quad (2.5)$$

$$c_2 \rightarrow c_2/\alpha^3, \quad (2.6)$$

$$c_3 \rightarrow c_3/\alpha^{1/2}, \quad (2.7)$$

$$c_4 \rightarrow c_4/\alpha, \quad (2.8)$$

$$Re_L \rightarrow \alpha Re_L. \quad (2.9)$$

We note that the above transformation is consistent with the relation  $Re_L = (2a)^2$  used above and allows for the transformation of the above set of coefficients to different Reynolds number definitions or aspect ratios. Such a new set of coefficients is obtained by first determining  $\alpha$ . Here  $\alpha$  is determined as  $Re_1(Ra, Pr)/Re_2(Ra, Pr)$ , where  $Re_1$  is the Reynolds number value of a measurement point in the data set at a given  $Ra$  and  $Pr$  and  $Re_2$  is the Reynolds number value obtained from the GL model with the coefficients mentioned above. Subsequently, equations (2.4)–(2.9) can be used to calculate the new coefficients.

In figures 3–5 we compare the original GL fit from Grossmann & Lohse (2001) with this new GL fit. These figures clearly reveal that the new GL fit is much closer to the data in the low- $Pr$  regime, while maintaining the similar excellent agreement for the high- $Pr$  data as before. We emphasize that this excellent agreement with all other presently available data from experiments and simulations confirms that the  $c_i$  and  $a$  values we calculated describes  $Nu(Ra, Pr)$  well in the regime that is nowadays covered by state-of-the-art experiments and simulations. It is also noteworthy that figures 3 and 4 show that the  $Nu$  number scaling with  $Ra$  is well-predicted by the GL theory for  $Ra$  values that are decades higher than the highest  $Ra$  point that is used to determine the  $c_i$  values, namely  $Ra = 2.25 \times 10^{10}$ , thus showing the predictive power of the GL theory.



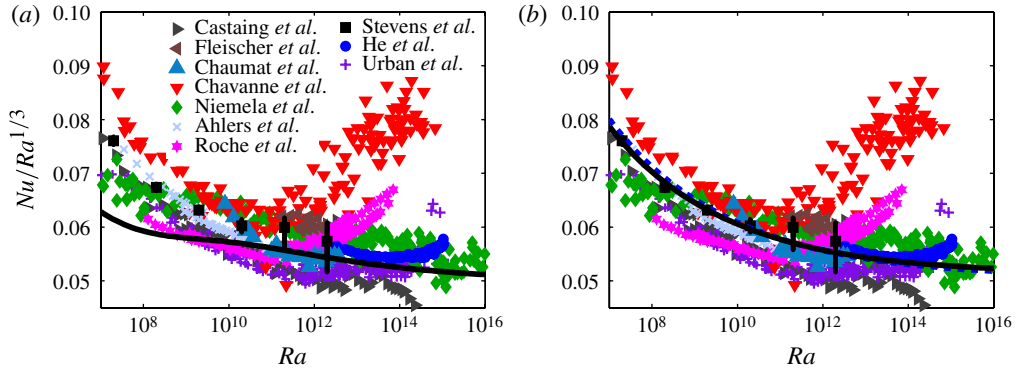


FIGURE 4. (Colour online) Comparison of the  $Ra$ -scaling of the original GL fit from Grossmann & Lohse (2001) (a) with the new fit (b) in a  $\Gamma = 1/2$  sample and varying  $Pr$ , see phase diagram in figure 8. The right pointing triangles are the experimental data from Castaing *et al.* (1989) with wall corrections Roche *et al.* (2010), left pointing triangles (Fleischer & Goldstein 2002), upward pointing triangles (Chaumat *et al.* 2002), downward pointing triangles (Chavanne *et al.* 2001), diamonds (Niemela *et al.* 2000), crosses (Ahlers *et al.* 2009a), hexagons (Roche *et al.* 2010), circles (Ahlers *et al.* 2012b; He *et al.* 2012b) and pluses (Urban, Musilová & Skrbek 2011; Urban *et al.* 2012) indicate experimental data and the squares results from numerical simulations (Stevens *et al.* 2010c, 2011a). The solid (black) line indicates the GL fit of § 2 and the dashed (shown in blue online) line the GL fit of § 3.

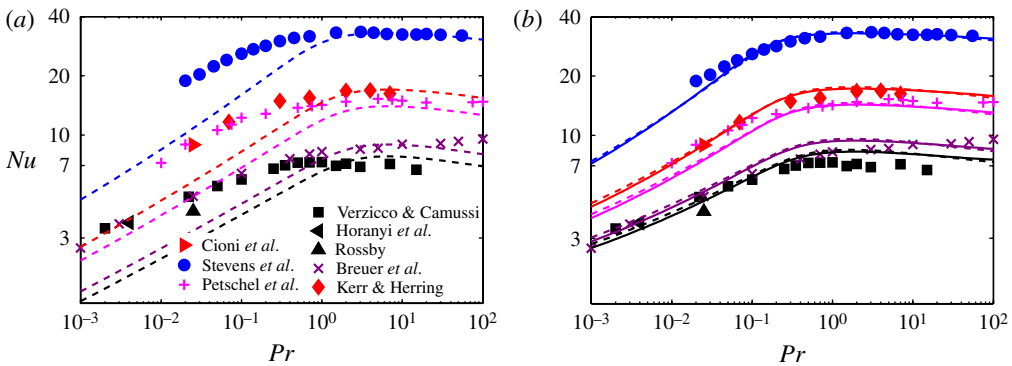


FIGURE 5. (Colour online) Comparison of the  $Pr$ -scaling of the original GL fit from Grossmann & Lohse (2001) (a) with the new fit (b) for different  $Ra$ . The right pointing triangle (Cioni *et al.* 1997), left pointing triangle (Horanyi, Krebs & Müller 1999) and the upward pointing triangle (Rosby 1969) indicate experimental results. The circles (van der Poel *et al.* 2013) and squares (Verzicco & Camussi 1999) indicate numerical results obtained in a cylinder with aspect ratio  $\Gamma = 1$ . The pluses (Petschel *et al.* 2013) indicate numerical results obtained in a periodic domain and the diamonds (Kerr & Herring 2000) and crosses (Breuer *et al.* 2004) numerical results obtained in a box with free slip boundary condition at the sidewall. The solid lines indicate the GL fit of § 2 and the dashed lines the GL fit in § 3. The lines from bottom to top (shown in colours black, purple, magenta, red and blue online, respectively) correspond to the  $Ra$  numbers  $5 \times 10^5$ ,  $10^6$ ,  $5 \times 10^6$ ,  $10^7$  and  $10^8$ .

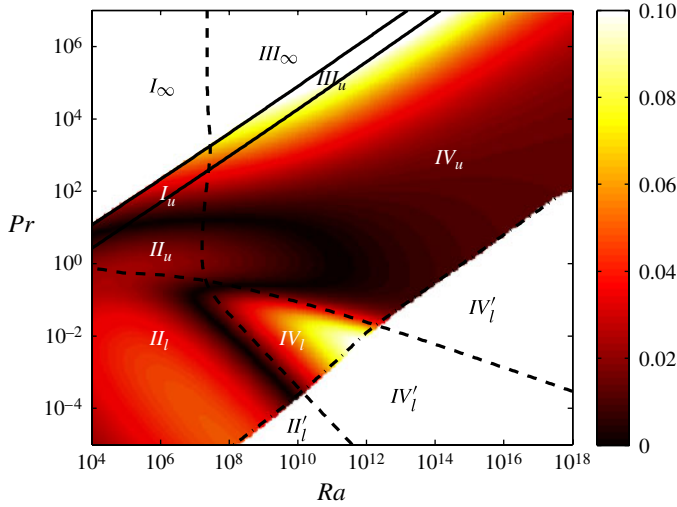


FIGURE 6. (Colour online) Relative difference between  $Nu$  calculated from the original fit and  $Nu$  calculated from the additional fit. The colour scale ranges from black to white, indicating agreement mostly up to  $\approx 4\%$ . Only in two small ranges,  $III_u$  and  $IV_l$ , does it go up to  $10\%$ .

### 3. Robustness

To illustrate the robustness of the fit presented above, we made a second fit to four other data points, i.e. the data points from Funfschilling *et al.* (2005) at  $Ra = 2.96 \times 10^7$  and  $Ra = 1.92 \times 10^{10}$  with  $Pr = 4.38$ , that from Xia *et al.* (2002) at  $Ra = 2.24 \times 10^8$  with  $Pr = 554$  and finally the data point by Kerr & Herring (2000) at  $Ra = 10^7$  with  $Pr = 0.07$ . Three out of these four data points lie relatively close to the original four data points, but the low  $Pr = 0.07$  point from Kerr & Herring (2000) substantially differs from the original  $Pr = 0.025$ . The reason that three of the four points are close to the original four points in the  $Ra$ – $Pr$  parameter space is that one can only select ‘reliable legs’ in regimes where many measurements have been done and these regimes only cover a limited part of the parameter space.

The resulting GL coefficients are  $c_1 = 11.8$ ,  $c_2 = 1.33$ ,  $c_3 = 0.528$ ,  $c_4 = 0.0222$  and  $a = 0.843$  compared with  $c_1 = 8.05$ ,  $c_2 = 1.38$ ,  $c_3 = 0.487$ ,  $c_4 = 0.0252$  and  $a = 0.922$  of the fit described above. In order to compare the two fits we show both fits together with experimental and numerical data from several experiments in figures 3, 4, 5 and 7. In addition we give the relative difference in  $Nu(Ra, Pr)$  calculated in the fit described in the previous section and  $Nu$  calculated from this additional fit in the parts of the parameter space where the GL fit is valid in figure 6. A comparison between both fits shows that the difference is very minor in the regimes  $IV_u$ ,  $II_u$  and  $I_u$ , and that the differences increase in the regimes  $II_l$ ,  $IV_l$  and  $III_u$ , which are very far away from the region in the parameter space where reliable data points are available. The reason is that a very small variation in the measurements point can lead to significant differences if the implied information is extrapolated over many decades in  $Ra$  and  $Pr$  using the GL theory. For the fits compared here the differences increase up to  $\sim 10\%$ . We find that the differences are mainly caused by the uncertainty in the Xia *et al.* (2002) data, which is reflected by the two different data points we took from this data set. In figure 7 we compare the Xia *et al.* (2002) measurements with the



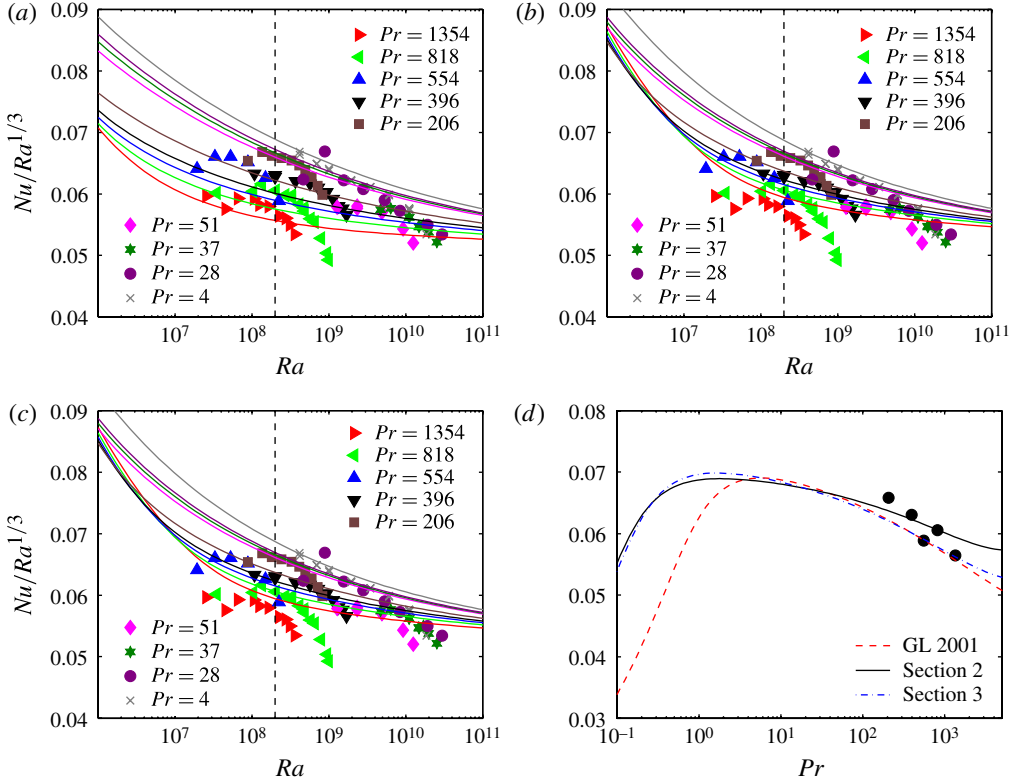


FIGURE 7. (Colour online) (a–c) The Nusselt number measurements of Xia *et al.* (2002) versus  $Ra$  in comparison with the original GL fit from Grossmann & Lohse (2001) (a), the GL fit presented in § 2 (b) and the second fit discussed in § 3 (c). (d) The  $Pr$  number dependence of the Xia *et al.* (2002) experiments for  $Ra \approx 2 \times 10^8$  compared with the three different GL fits mentioned above.

original GL fit from Grossmann & Lohse (2001), and the two fits presented in this work. Figure 7(a–c) show that the measured  $Nu/Ra^{1/3}$  decreases faster with increasing  $Ra$  than predicted by the GL model. A comparison of the Xia *et al.* (2002) data with other data obtained at  $Pr = 4.38$  shows that the measurements in the lower- $Ra$  regime collapse very well with other measurements, while for the higher  $Ra$  the measured Nusselt number seems a little lower in the Xia *et al.* (2002) experiments than in other experiments. Figure 7(d) compares the Xia *et al.* (2002) measurements between  $Ra \approx 2 \times 10^8$  and  $Ra \approx 2.4 \times 10^8$  with the different GL fits and shows that the fit presented in § 2 uses a high- $Pr$  point that aligns with the reliable  $Pr = 4.38$  data point, while the second fit uses a high- $Pr$  point of the lower branch. In this way the uncertainty of these measurements is reflected by the two fits and as is shown in figure 6 this difference is mostly visible near regime  $I_\infty$  and  $III_\infty$ .

#### 4. GL theory for $\Gamma = 1/2$ and ultimate regime

In principle, the  $c_i$  depend on the aspect ratio  $\Gamma$ . However, it is well-known that only small differences in  $Nu$  are observed between  $\Gamma = 1/2$  and  $\Gamma = 1$  (Ahlers *et al.* 2009b). This weak aspect ratio dependence is confirmed by figure 4, which shows that

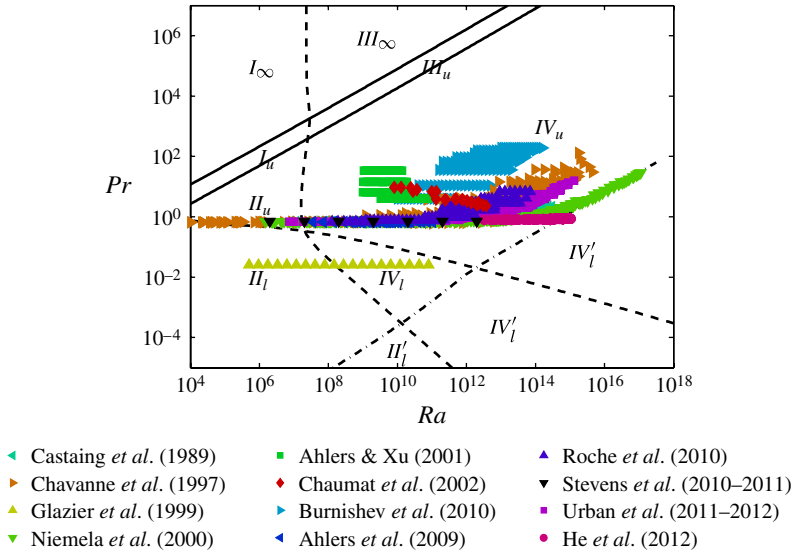


FIGURE 8. (Colour online) Phase diagram in  $Ra$ - $Pr$  plane for RB convection in a  $\Gamma = 1/2$  sample with no-slip boundary conditions. The lines are the same as in figure 1. The data are from Castaing *et al.* (1989), Chavanne *et al.* (1997), Glazier *et al.* (1999), Niemela *et al.* (2000), Ahlers & Xu (2001), Chaumat *et al.* (2002), Ahlers *et al.* (2009*b*), Burnishev *et al.* (2010), Roche *et al.* (2010), Urban *et al.* (2011), Urban *et al.* (2012), He *et al.* (2012*b*) and Stevens *et al.* (2010*c*, 2011*a*).

the  $Ra$  number scaling for  $Pr = 0.7$  in a  $\Gamma = 1/2$  sample is captured very accurately by the new fit for  $\Gamma = 1$ , and in the low- $Ra$  number regime the new fit is even much better than the original GL fit from Grossmann & Lohse (2001).

The location in  $Ra$ - $Pr$  space of the various regimes of the GL theory is based on the coefficients  $c_i$  and  $a$ . The updated lines that encompass the regimes are plotted in the phase diagrams shown in figures 1 and 8. The line that indicates the onset of the ultimate regime, where the kinetic BL has become turbulent, is now based on the new coefficients, the transition at  $Ra = 5 \times 10^{14}$ , observed by He *et al.* (2012*b*) for  $Pr = 0.86$ , and the  $Re$  number measurements by Qiu & Tong (2001). This gives  $Re_s^* = 1039$  ( $a = 0.922$ ) and for the second fit we made, see § 3, we get  $Re_s^* = 954$  ( $a = 0.843$ ). In a  $\Gamma = 1/2$  sample He *et al.* (2012*b*) found experimentally that  $Re = 0.252Ra^{0.434}Pr^{0.750}$  using a recently developed and tested elliptic approximation (He & Zhang 2006; Zhao & He 2009; He, He & Tong 2010; He & Tong 2011; Zhou *et al.* 2011), which defines  $Re$  unambiguously, based on properties of correlation functions. Using this relation at  $Ra = 10^{13}$  and  $Pr = 0.86$  this gives  $Re_s^* = 572$  with  $a = 0.684$  for the first fit, see § 2, and  $Re_s^* = 521$  with  $a = 0.623$  for the second fit we made, see § 3. These  $Re_s^*$  values are different from the previously used  $Re_s^* = 420$  with  $a = 1.72$  taken from pipe flow (Landau & Lifshitz 1987). From the transformation property of the GL equations one gets that  $Re_s^*$  increases by a factor of  $\alpha$  when  $Re$  increases by a factor  $\alpha$ , while  $a$  increases by a factor  $\sqrt{\alpha}$ . The  $a$  values found here are significantly different from  $a = 0.482$ , which was found by Grossmann & Lohse (2002). Calculating the  $Re_s^*$  values equivalent to  $a = 0.482$  from the  $a$  and  $Re_s$  combinations mentioned above, i.e.  $a = 0.843$  with  $Re_s^* = 954$ ,  $a = 0.922$  with  $Re_s^* = 1039$ ,  $a = 0.684$  with  $Re_s^* = 572$  and  $a = 0.623$  with  $Re_s^* = 521$

gives  $Re_s^* = 298 \pm 15$  for the new coefficients, so we see that the notification of  $Re_s^*$  alone, without  $a$ , is not sufficient.

The phase diagram in figure 8 shows that the measurements of He *et al.* (2012*b*) up to  $Ra \approx 10^{15}$  at  $Pr = 0.86$  are up to now the only experiments that have reached the ultimate regime. They observe the onset of the ultimate regime at  $Ra = 5 \times 10^{14}$  and a transition region for  $10^{13} \leq Ra \leq 5 \times 10^{14}$ . The experiments by He *et al.* (2012*b*) are the only room-temperature experiments for  $Ra \gtrsim 10^{12}$ , while all other experiments that have reached these  $Ra$  numbers are low-temperature experiments with helium close to the critical point (Chavanne *et al.* 1997, 2001; Niemela *et al.* 2000, 2001; Niemela & Sreenivasan 2006; Roche *et al.* 2010; Urban *et al.* 2011, 2012). In these low-temperature experiments it is difficult to reach the ultimate regime because the  $Pr$  number increases with increasing  $Ra$ , see figure 8. Nevertheless the low-temperature experiments by Niemela *et al.* (2000) seem to come very close to the ultimate regime and one may wonder why the transition region observed by He *et al.* (2012*b*) was not observed in the Niemela *et al.* (2000) experiments. As discussed in detail by Ahlers *et al.* (2012*b*), presumably the scatter of the Niemela *et al.* (2000) data at this highest  $Ra$  (which seems to be due primarily to the uncertainties in the fluid properties) as well as the fact that the transition is smooth are the reasons for this. Figure 4 shows that the magnitude of the scatter in the Niemela *et al.* (2000) data is similar to the observed increase in the compensated Nusselt number in the transition regime by He *et al.* (2012*b*). The phase diagram also shows that other low-temperature experiments by Chavanne *et al.* (1997, 2001), Roche *et al.* (2010) and Urban *et al.* (2011, 2012) do not reach the ultimate regime and therefore no transition to the ultimate regime due to a BL shear instability is expected in these experiments.

## 5. Conclusions and outlook

In this paper we have used the availability of new experimental and numerical data, and our increased understanding of the physics of the Rayleigh–Bénard system to determine the prefactors of the unifying theory for scaling in thermal convection, i.e. the GL theory, much more accurately. The resulting  $Nu(Ra, Pr)$  function is in very good agreement with almost all established experimental and numerical data up to the ultimate regime of thermal convection, and has significantly improved the predictions. In figure 4 one can notice the onset of the ultimate regime in the  $Nu(Ra)$  scaling of the measurements of He *et al.* (2012*b*). Extensions of the GL theory to the ultimate regime by Grossmann & Lohse (2011) are able to explain the observed Reynolds number scaling in that regime as well as the origin of the log-profiles observed in the ultimate regime by Ahlers *et al.* (2012*a*).

In line with Grossmann & Lohse (2001), we have determined the prefactors from experimental measurements. This has great value as it shows that the information of only five data points is sufficient to accurately predict  $Nu(Ra, Pr)$  and  $Re(Ra, Pr)$  up to the ultimate regime. This is based on the GL theory, which builds on exact global balances for the energy and thermal dissipation rates, derived from the Boussinesq equations, and the decomposition of the flow in BL and bulk contributions. A finding with further implications is that the value  $a$ , i.e. the amplitude parameter of the Prandtl BL thickness, is higher than that found by Grossmann & Lohse (2002). This  $a$  value is for example used by Shishkina *et al.* (2010) to determine the number of grid points that should be placed in the BLs. Shishkina *et al.* (2010) compared the theoretical predictions with results from simulations in  $\Gamma = 1/2$  samples. For this aspect ratio the newly found value of  $a$  ( $a = 0.684$  for fit of § 2 and  $a = 0.623$  of § 3) is higher, but

still relatively close to the previously used  $a = 0.482$ . However, for the  $\Gamma = 1$  case it looks like  $a$  is even higher ( $a = 0.922$  for the fit of § 2 and  $a = 0.843$  for the fit of § 3), which could have implications for the resolution that should be used in simulations. This finding confirms the conclusions of Stevens *et al.* (2010c) who pointed out that the only way to really confirm that the used numerical resolution is sufficient is to obtain the same Nusselt number with different grids resolutions as there is namely always some uncertainty in estimates of the required grid resolution.

A further challenge we want to pursue is to calculate the  $c_i$  and  $a$  directly from the fluid equations, without the input of any experimental or numerical data, or at least quantitatively relate their values to important fluid concepts such as Prandtl–Blasius–Pohlhausen theory, the von Kármán–Prandtl theory, etc. in order to get an even deeper understanding of the GL theory.

### Acknowledgements

We thank all of our colleagues for various discussions over the years and G. Ahlers, F. Chilla, K. Petschel, P. Roche, L. Skrbek, R. Verzicco and K.-Q. Xia for providing us with their experimental and numerical data and for numerous scientific discussions and insightful remarks on RB over the years. Special thanks go to G. Ahlers for his insightful comments on earlier versions of this manuscript. We acknowledge the Foundation for Fundamental Research of Matter (FOM), which is part of NWO, for funding.

### REFERENCES

- AHLERS, G. 2000 Effect of sidewall conductance on heat-transport measurements for turbulent Rayleigh–Bénard convection. *Phys. Rev. E* **63**, 015303.
- AHLERS, G., BODENSCHATZ, E., FUNFSCHILLING, D., GROSSMANN, S., HE, X., LOHSE, D., STEVENS, R. J. A. M. & VERZICCO, R. 2012a Logarithmic temperature profiles in turbulent Rayleigh–Bénard convection. *Phys. Rev. Lett.* **109**, 114501.
- AHLERS, G., BODENSCHATZ, E., FUNFSCHILLING, D. & HOGG, J. 2009a Turbulent Rayleigh–Bénard convection for a Prandtl number of 0.67. *J. Fluid Mech.* **641**, 157–167.
- AHLERS, G., GROSSMANN, S. & LOHSE, D. 2009b Heat transfer and large-scale dynamics in turbulent Rayleigh–Bénard convection. *Rev. Mod. Phys.* **81**, 503–537.
- AHLERS, G., HE, X., FUNFSCHILLING, D. & BODENSCHATZ, E. 2012b Heat transport by turbulent Rayleigh–Bénard convection for  $Pr = 0.8$  and  $3 \times 10^{12} \leq Ra \leq 10^{15}$ : aspect ratio  $\Gamma = 0.50$ . *New J. Phys.* **14**, 063030.
- AHLERS, G. & XU, X. 2001 Prandtl-number dependence of heat transport in turbulent Rayleigh–Bénard convection. *Phys. Rev. Lett.* **86**, 3320–3323.
- BREUER, M., WESSLING, S., SCHMALZL, J. & HANSEN, U. 2004 Effect of inertia in Rayleigh–Bénard convection. *Phys. Rev. E* **69**, 026302.
- BROWN, E., FUNFSCHILLING, D., NIKOLAENKO, A. & AHLERS, G. 2005 Heat transport by turbulent Rayleigh–Bénard convection: effect of finite top- and bottom conductivity. *Phys. Fluids* **17**, 075108.
- BURNISHEV, Y., SEGRE, E. & STEINBERG, V. 2010 Strong symmetrical non-Oberbeck–Boussinesq turbulent convection and the role of compressibility. *Phys. Fluids* **22**, 035108.
- CASTAING, B., GUNARATNE, G., HESLOT, F., KADANOFF, L., LIBCHABER, A., THOMAE, S., WU, X. Z., ZALESKI, S. & ZANETTI, G. 1989 Scaling of hard thermal turbulence in Rayleigh–Bénard convection. *J. Fluid Mech.* **204**, 1–30.
- CHAUMAT, S., CASTAING, B. & CHILLA, F. 2002 Rayleigh–Bénard cells: influence of plate properties. In *Advances in Turbulence IX* (ed. I. P. Castro, P. E. Hancock & T. G. Thomas). International Center for Numerical Methods in Engineering, CIMNE.

- CHAVANNE, X., CHILLA, F., CASTAING, B., HEBRAL, B., CHABAUD, B. & CHAUSSY, J. 1997 Observation of the ultimate regime in Rayleigh–Bénard convection. *Phys. Rev. Lett.* **79**, 3648–3651.
- CHAVANNE, X., CHILLA, F., CHABAUD, B., CASTAING, B. & HEBRAL, B. 2001 Turbulent Rayleigh–Bénard convection in gaseous and liquid He. *Phys. Fluids* **13**, 1300–1320.
- CIONI, S., CILIBERTO, S. & SOMMERIA, J. 1997 Strongly turbulent Rayleigh–Bénard convection in mercury: comparison with results at moderate Prandtl number. *J. Fluid Mech.* **335**, 111–140.
- EMRAN, M. S. & SCHUMACHER, J. 2012 Conditional statistics of thermal dissipation rate in turbulent Rayleigh–Bénard convection. *Eur. Phys. J. E* **108**, 35–42.
- FLEISCHER, A. S. & GOLDSTEIN, R. J. 2002 High-Rayleigh-number convection of pressurized gases in a horizontal enclosure. *J. Fluid Mech.* **469**, 1–12.
- FUNFSCHILLING, D., BROWN, E., NIKOLAENKO, A. & AHLERS, G. 2005 Heat transport by turbulent Rayleigh–Bénard convection in cylindrical cells with aspect ratio one and larger. *J. Fluid Mech.* **536**, 145–154.
- GLAZIER, J. A., SEGAWA, T., NAERT, A. & SANO, M. 1999 Evidence against ultrahard thermal turbulence at very high Rayleigh numbers. *Nature* **398**, 307–310.
- GROSSMANN, S. & LOHSE, D. 2000 Scaling in thermal convection: a unifying view. *J. Fluid Mech.* **407**, 27–56.
- GROSSMANN, S. & LOHSE, D. 2001 Thermal convection for large Prandtl number. *Phys. Rev. Lett.* **86**, 3316–3319.
- GROSSMANN, S. & LOHSE, D. 2002 Prandtl and Rayleigh number dependence of the Reynolds number in turbulent thermal convection. *Phys. Rev. E* **66**, 016305.
- GROSSMANN, S. & LOHSE, D. 2004 Fluctuations in turbulent Rayleigh–Bénard convection: the role of plumes. *Phys. Fluids* **16**, 4462–4472.
- GROSSMANN, S. & LOHSE, D. 2011 Multiple scaling in the ultimate regime of thermal convection. *Phys. Fluids* **23**, 045108.
- HE, X., FUNFSCHILLING, D., BODENSCHATZ, E. & AHLERS, G. 2012a Heat transport by turbulent Rayleigh–Bénard convection for  $Pr = 0.8$  and  $4 \times 10^{11} \leq Ra \leq 2 \times 10^{14}$  for aspect ratio  $\Gamma = 1.00$ . *New J. Phys.* **14**, 103012.
- HE, X., FUNFSCHILLING, D., NOBACH, H., BODENSCHATZ, E. & AHLERS, G. 2012b Transition to the ultimate state of turbulent Rayleigh–Bénard convection. *Phys. Rev. Lett.* **108**, 024502.
- HE, X., HE, G. & TONG, P. 2010 Small-scale turbulent fluctuations beyond Taylor’s frozen-flow hypothesis. *Phys. Rev. E* **81**, 065303.
- HE, X. & TONG, P. 2011 Kraichnan’s random sweeping hypothesis in homogeneous turbulent convection. *Phys. Rev. E* **83**, 037302.
- HE, G. W. & ZHANG, J. B. 2006 Elliptic model for space–time correlations in turbulent shear flows. *Phys. Rev. E* **73**, 055303.
- HORANYI, S., KREBS, L. & MÜLLER, U. 1999 Turbulent Rayleigh–Bénard convection in low Prandtl number fluids. *Int. J. Heat Mass Transfer* **42**, 3983–4003.
- KERR, R. & HERRING, J. R. 2000 Prandtl number dependence of Nusselt number in direct numerical simulations. *J. Fluid Mech.* **419**, 325–344.
- LAKKARAJU, R., STEVENS, R. J. A. M., VERZICCO, R., GROSSMANN, S., PROSPERETTI, A., SUN, C. & LOHSE, D. 2012 Spatial distribution of heat flux and fluctuations in turbulent Rayleigh–Bénard convection. *Phys. Rev. E* **86**, 056315.
- LANDAU, L. D. & LIFSHITZ, E. M. 1987 *Fluid Mechanics*. Pergamon.
- LOHSE, D. & XIA, K. Q. 2010 Small-scale properties of turbulent Rayleigh–Bénard convection. *Annu. Rev. Fluid Mech.* **42**, 335–364.
- NIEMELA, J., SKRBEK, L., SREENIVASAN, K. R. & DONNELLY, R. 2000 Turbulent convection at very high Rayleigh numbers. *Nature* **404**, 837–840.
- NIEMELA, J., SKRBEK, L., SREENIVASAN, K. R. & DONNELLY, R. J. 2001 The wind in confined thermal turbulence. *J. Fluid Mech.* **449**, 169–178.
- NIEMELA, J. & SREENIVASAN, K. R. 2003 Confined turbulent convection. *J. Fluid Mech.* **481**, 355–384.
- NIEMELA, J. & SREENIVASAN, K. R. 2006 Turbulent convection at high Rayleigh numbers and aspect ratio 4. *J. Fluid Mech.* **557**, 411–422.

- PETSCHER, K., STELLMACH, S., WILCZEK, M., LÜLFF, J. & HANSEN, U. 2013 Dissipation layers in Rayleigh–Bénard convection: a unifying view. *Phys. Rev. Lett.* **110**, 114502.
- QIU, X. L. & TONG, P. 2001 Large scale velocity structures in turbulent thermal convection. *Phys. Rev. E* **64**, 036304.
- ROCHE, P. E., CASTAING, B., CHABAUD, B., HEBRAL, B. & SOMMERIA, J. 2001 Side wall effects in Rayleigh–Bénard experiments. *Eur. Phys. J. B* **24**, 405–408.
- ROCHE, P.-E., GAUTHIER, F., KAISER, R. & SALORT, J. 2010 On the triggering of the ultimate regime of convection. *New J. Phys.* **12**, 085014.
- ROSSBY, H. T. 1969 A study of Bénard convection with and without rotation. *J. Fluid Mech.* **36**, 309–335.
- SCHLICHTING, H. 1979 *Boundary Layer Theory*, 7th edn. McGraw-Hill.
- SHISHKINA, O., STEVENS, R. J. A. M., GROSSMANN, S. & LOHSE, D. 2010 Boundary layer structure in turbulent thermal convection and its consequences for the required numerical resolution. *New J. Phys.* **12**, 075022.
- SHISHKINA, O. & TCESS, A. 2009 Mean temperature profiles in turbulent Rayleigh–Bénard convection of water. *J. Fluid Mech.* **633**, 449–460.
- SIGGIA, E. D. 1994 High Rayleigh number convection. *Annu. Rev. Fluid Mech.* **26**, 137–168.
- STEVENS, R. J. A. M., CLERCX, H. J. H. & LOHSE, D. 2010a Boundary layers in rotating weakly turbulent Rayleigh–Bénard convection. *Phys. Fluids* **22**, 085103.
- STEVENS, R. J. A. M., CLERCX, H. J. H. & LOHSE, D. 2010b Optimal Prandtl number for heat transfer in rotating Rayleigh–Bénard convection. *New J. Phys.* **12**, 075005.
- STEVENS, R. J. A. M., LOHSE, D. & VERZICCO, R. 2011a Prandtl number dependence of heat transport in high Rayleigh number thermal convection. *J. Fluid Mech.* **688**, 31–43.
- STEVENS, R. J. A. M., OVERKAMP, J., LOHSE, D. & CLERCX, H. J. H. 2011b Effect of aspect-ratio on vortex distribution and heat transfer in rotating Rayleigh–Bénard convection. *Phys. Rev. E* **84**, 056313.
- STEVENS, R. J. A. M., VERZICCO, R. & LOHSE, D. 2010c Radial boundary layer structure and Nusselt number in Rayleigh–Bénard convection. *J. Fluid Mech.* **643**, 495–507.
- SUN, C., REN, L.-Y., SONG, H. & XIA, K.-Q. 2005 Heat transport by turbulent Rayleigh–Bénard convection in 1m diameter cylindrical cells of widely varying aspect ratio. *J. Fluid Mech.* **542**, 165–174.
- SUN, C. & XIA, K.-Q. 2005 Scaling of the Reynolds number in turbulent thermal convection. *Phys. Rev. E* **72**, 067302.
- URBAN, P., HANZELKA, P., KRÁLIK, T., MUSILOVA, V., SRNKA, A. & SKRBK, L. 2012 Effect of boundary layers asymmetry on heat transfer efficiency in turbulent Rayleigh–Bénard convection at very high Rayleigh numbers. *Phys. Rev. Lett.* **109**, 154301.
- URBAN, P., MUSILOVÁ, V. & SKRBK, L. 2011 Efficiency of heat transfer in turbulent Rayleigh–Bénard convection. *Phys. Rev. Lett.* **107**, 014302.
- VAN DER POEL, E. P., STEVENS, R. J. A. M. & LOHSE, D. 2013 Comparison between two and three-dimensional Rayleigh–Bénard convection. *J. Fluid Mech.* (Submitted).
- VERZICCO, R. 2002 Sidewall finite conductivity effects in confined turbulent thermal convection. *J. Fluid Mech.* **473**, 201–210.
- VERZICCO, R. & CAMUSSI, R. 1999 Prandtl number effects in convective turbulence. *J. Fluid Mech.* **383**, 55–73.
- XIA, K.-Q., LAM, S. & ZHOU, S. Q. 2002 Heat-flux measurement in high-Prandtl-number turbulent Rayleigh–Bénard convection. *Phys. Rev. Lett.* **88**, 064501.
- ZHAO, X. & HE, G.-W. 2009 Space–time correlations of fluctuating velocities in turbulent shear flows. *Phys. Rev. E* **79**, 046316.
- ZHOU, Q., LI, C.-M., LU, Z.-M. & LIU, Y.-L. 2011 Experimental investigation of longitudinal space–time correlations of the velocity field in turbulent Rayleigh–Bénard convection. *J. Fluid Mech.* **683**, 94–111.